A Gold Nanoparticle Functionalized Reverse Thermal Gel for Tissue Engineering Applications.

Brisa Peña[1,2], Marcos Maldonado[3], Andrew J. Bonham[3], Brian A. Aguado[4], Antonio Dominguez-Alfaro[5,6], Melissa Laughter[2], Teisha J. Rowland[1], James Bardill[2], Nikki L. Farnsworth[2], Nuria Alegret Ramon[1,6], Matthew R. G. Taylor[1], Kristi S. Anseth[4], Maurizio Prato[5, 7,8], Robin Shandas[2], Timothy A. McKinsey[1,9], Daewon Park[2] and Luisa Mestroni[1]*.*

KEYWORDS. Cardiac Tissue Engineering, Reverse Thermal Gel, Gold Nanoparticles, Injectable Polymer, Tissue Engineering.

AUTHOR ADDRESS

[1] Department of Medicine, Division of Cardiology, University of Colorado Anschutz Medical Campus, at 12700 E.19th Avenue, Bldg. P15, Aurora, Colorado, 80045, United States.

[2] Bioengineering Department, University of Colorado Denver Anschutz Medical Campus, at Bioscience 2 1270 E. Montview Avenue, Suite 100, Aurora, Colorado, 80045, United States.

[3]Department of Chemistry, Metropolitan State University of Denver, at 1201 5th St, Denver, Colorado, 80206, United States.

[4] Department of Chemical and Biological Engineering and the BioFrontiers Institute, University of Colorado at Boulder, 3415 Colorado Avenue, Boulder, Colorado, 80309, United States.

[5] Carbon Nanobiotechnology Laboratory CIC biomaGUNE, Paseo de Miramón 182 20009 Donostia-San Sebastián, 20009, Spain.

[6] POLYMAT, University of the Basque Country UPV/EHU, Avenida de Tolosa 72, 20018 Donostia-San Sebastián, Spain.

[7] Department of Chemical and Pharmaceutical Sciences, University of Trieste, Via Giorgieri 1, Trieste, 34127, Italy.

[8] Basque Fdn Sci, Ikerbasque, Bilbao 48013, Spain.

[9] Consortium for Fibrosis Research & Translation, University of Colorado Anschutz Medical Campus, Aurora, CO 80045, United States.

ABSTRACT. Utilizing polymers in cardiac tissue engineering holds promise for restoring function to the heart following myocardial infarction (MI), which is associated with grave morbidity and mortality. To properly mimic native cardiac tissue, materials must not only support cardiac cell growth but also have inherent conductive properties. Here, we present an injectable reverse thermal gel (RTG)-based cardiac cell scaffold system that is both biocompatible and conductive. Following synthesis of a highly-functionalizable, biomimetic RTG backbone, gold nanoparticles (AuNPs) were chemically conjugated to the backbone to enhance the system's conductivity. The resulting RTG-AuNPs hydrogel supported targeted survival of neonatal rat ventricular myocytes (NRVMs) for up to 21 days when co-cultured with cardiac fibroblasts, leading to an increase in Cx43 relative to control cultures (NRVMs cultured on traditional gelatin-coated dishes and RTG hydrogel without AuNPs). This biomimetic and conductive RTG-AuNPs hydrogel holds promise for future cardiac tissue engineering applications.

Introduction. Post-myocardial infarction (MI) cardiomyocyte loss triggers matrix degradation and fibrosis that drives the progression to heart failure (HF)[1–3]. HF leads to a poor quality of life and an increased risk of mortality[4]. Heart transplantation remains the gold standard treatment for those with end-stage HF, but availability of donor hearts is a major limitation[5–7]. Due to the limited supply of donor hearts and the limited regenerative ability of the myocardium, there is an urgent need for novel treatment approaches following MI. Investigators have focused on the development of biomaterials aimed at supporting the infarct site and overall restoring cardiac function[8–12].

Injectable hydrogels provide a particularly attractive approach for MI treatment due to their potential to be delivered in a minimally invasive manner, thus minimizing mechanical stress on

the cells during injection and at the infarcted area, while providing structural support for the infarct[13–15]. In addition, due to the 3D nature of these platforms, they better mimic the *in vivo* microenvironment than 2D platforms[16]. Compared to other injectable hydrogels, reverse thermal gel (RTG) systems in particular are advantageous in that they undergo a reversible solution-to-gelation (sol-to-gel) transition solely through temperature stimuli[17], a less harmful process for encapsulated cells and tissue than systems that require UV radiation for crosslinking, which can generate oxidative damage to DNA[18].

Because native cardiac tissue has unique electrophysiological behavior that is critical for the transfer of electrical signals and function of cardiomyocytes (CMs)[19], an ideal hydrogel system would be conductive, supporting electrical signaling between cells. While injectable hydrogels hold great potential for use in cardiac tissue engineering, the majority of them are electrically insulated[20]. To improve the electrical properties of injectable hydrogels, investigators have modified these hydrogels through chemical conjugation or mixing with conductive nanoparticles, such as gold nanoparticles (AuNPs)[21–27]. AuNPs are highly conductive biocompatible biostructures[25] that confer conductive properties to otherwise inert cells.

Previously, we developed an injectable and highly biocompatible RTG designed to promote long-term CM survival[28]. This RTG consists of poly(serinol hexamethylene urea)-co-poly(N-isopropylacrylamide) functionalized with lysine, termed "RTG-lysine". The RTG-lysine hydrogel contains several free amine groups for functionalization which are useful for a wide variety of bio-conjugations[29–33]. Here, we used the free amine groups of the RTG-lysine system to chemically conjugate AuNPs functionalized with carboxylic acid (COOH) groups, creating a novel RTG-AuNPs hydrogel. We found that CMs co-cultured with cardiac fibroblasts (CFs) had improved long-term viability, cardiac marker expression and increased Cx43 area when cultured in the 3D

RTG-AuNPs hydrogel compared to standard 2D culture systems and the unmodified RTG (hydrogel without AuNPs).

Material and Methods.

Materials. Materials were purchased and prepared as previously described[34], except for the following materials. Auric chloride ($HAuCl_4$), trisodium citrate, sodium nitrate, sodium chloride, and 4-mercaptobutryic acid were purchased from Sigma-Aldrich and used as received. Water was purified using a Barnstead MicroPure system (Thermo Fisher).

Equipment. AuNP size was estimated via both UV/Vis spectroscopy and transmission electron microscopy (TEM). UV/Vis readings were collected using a Nanodrop 2000 spectrophotometer (ThermoFisher). TEM analyses were performed by dispersing AuNPs onto formvar-coated copper grids followed by interrogation using a JEOL JSM-1400plus TEM operated at 120 kV. Thermogravimetric analyses (TGA) were carried out as previously described[34], except that the decreased nitrogen flow used here was (25 mL/min). Resistance, viscosity, and mechanical (storage and loss moduli) analyses were conducted as previously described[34], with the following exceptions. For resistance and viscosity measurements, a 3% (w/w) polymer solution was used. Mechanical properties were determined using a constant angular frequency of 0.5 rad/s at 1.0% stain. Frequency sweep analysis was performed using an 8 mm parallel plate geometry with frequency sweeps ranging from 0.1 to 10 rad/sec (20 points per decade collected). The dynamic decay of C, N, O and Au was performed using a SPECS SAGE HR 100 system spectrometer (Sage). A Mg Kα (1253.6 eV) X-ray source at 12.5 kV and 10 mA was used for the analysis with a take-off angle of 90° and operating pressure of 8×10^{-8} mbar. Quantitative spectral analysis was

performed with the Casa X-ray photoelectron spectroscopy (XPS) 2.3 software. Morphological characterization of a 3% (w/w) RTG-AuNP solution was performed using a JSM-6010LA scanning electron microscope (SEM) (JEOL, Tokyo, Japan), as previously described[34], using cryogenic horizontal and vertical cuts with an approximate width of 2 mm. 3D and 2D cell cultures were imaged using a Zeiss-LSM780 confocal microscope.

Preparation of Citrate Stabilized Gold Nanoparticles (AuNPs). Glassware used for the synthesis of AuNPs was cleaned using aqua regia (3:1 HCl: HNO_3), rinsed with Barnstead water, and allowed to air dry. AuNPs were prepared by mixing 5 mL of 0.01 M $HAuCl_4$, 20 mL of 0.01 M sodium citrate, and 25 mL of Barnstead water. The solution was refluxed until a deep red color developed and then was allowed to cool to room temperature. The resulting AuNPs were concentrated to approximately 10 nM in pH 11 water. AuNP functionalization was carried out by adding 1 mL of 10 nM 4-mercaptobutyric acid per 10 mL aliquot of AuNPs. Excess acid was removed by aging the solution in salt up to a concentration of 3.6 mM NaCl. AuNPs were resuspended to a final concentration of 10 nM in pH 11 water.

Polymer Synthesis. AuNPs were conjugated to RTG-lysine, which was synthesized as previously described[28,34], by dissolving 10nM of AuNPs-COOH in 15 mL of PBS. Five molar excess of EDC-HCl/NHS was added to activate the COOH groups (15 min at room temperature). Then 5 mL of RTG-lysine in solution (0.1 g/mL) prepared in PBS was added drop-wise and the reaction carried out for 48 h at RT. The RTG-AuNPs polymer was then dialyzed, lyophilized, and underwent L-Lysine addition as previously described[34]. The final polymer was dialyzed, sterile-filtered through a 2 μm filter, and lyophilized, previously described[34].

Neonatal rat ventricular myocyte (NRVM) culture. Primary NRVMs were prepared from 1-3 day old, Sprague Dawley rat pups (Charles River), as previously described[34–36] according to the University of Colorado Denver Animal Care and Use Committee guidelines. The resultant NRMVs were cultured in 2D gelatin-coated plates (2D gelatin controls) or in the 3D hydrogels.

3D *in vitro* cell culture. 3D *in vitro* culture experiments were performed as previously reported[34]. Briefly, NRVMs ($9x10^4$) were pelleted, media aspirated, and the cell pellet mixed with room temperature polymeric solution (150 µL of 3% [w/w]) dissolved in complete media. The cell-polymer solution was deposited into a glass bottom dish and incubated at 37 °C for 15 min at 5% CO_2, which allows gel formation. Following incubation, warm media (200 µL) was deposited on top of the solidified gel with encapsulated cells. **Scheme 1** shows the schematic representation of the 3D cell culture.

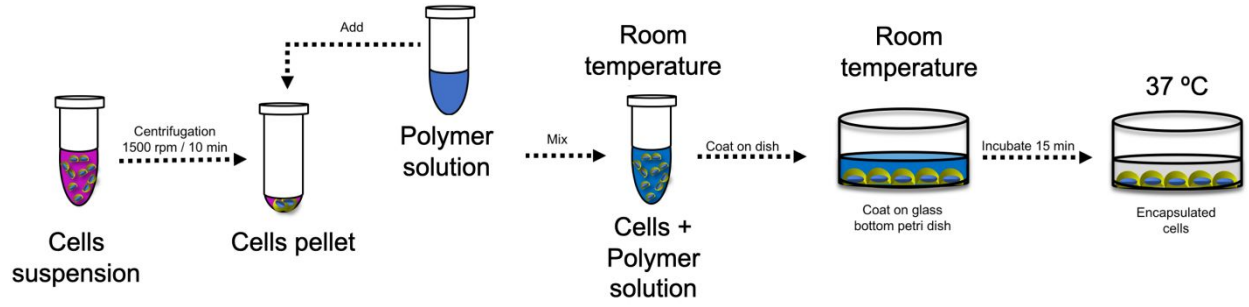

Scheme 1. Representation of the 3D cell culture method using the RTG hydrogels.

Immunocytochemistry. Immunocytochemistry was performed as previously described[34], using cells cultured for 21 days[34] and primary antibodies against alpha actinin (Abcam ab9465, at 1:100), Cx43 (SIGMA c6219, at 1:100), and vimentin (Abcam ab24525, at 1;100). Goat anti-mouse conjugated to Alexa Fluor 488 (Invitrogen, at 1:200), goat anti-rabbit conjugated to TRITC

(Sigma, at 1:200), and goat anti-chicken Cy5 (Abcam, at 1:200) were used as secondary antibodies. Cell nuclei were stained with DAPI (1:2000).

Statistical analysis. Data were collected in triplicate from ≥3 independent experiments. Statistical significance was calculated and determined using ANOVA. P-values <0.05 were considered statistically significant.

Results

RTG-AuNP synthesis. Using our previously established RTG-lysine as a platform[28], here we developed a novel 3D RTG-AuNP hydrogel. The objective of this system was to provide (1) a conductive, low viscous injectable hydrogel that (2) supports long-term survival of co-cultured CMs and CFs. First, we synthetized AuNPs with COOH functional groups (**Figure 1A**), which are easily dispersed in water (**Figure S1A**). Next, the size and morphological characterization of the AuNPs-COOH was analyzed by both UV/Vis spectroscopy and TEM (**Figure 1B and Figure 1C**). UV/Vis readings showed a surface plasmon absorbance peak at 528 nm, indicating an AuNPs-COOH size of approximately 35 nm diameter (**Figure 1B**). Using TEM analysis, the AuNPs-COOH were shown to have a rounded morphology with an approximate average diameter of 32 +/- 8 nm (**Figure 1C**).

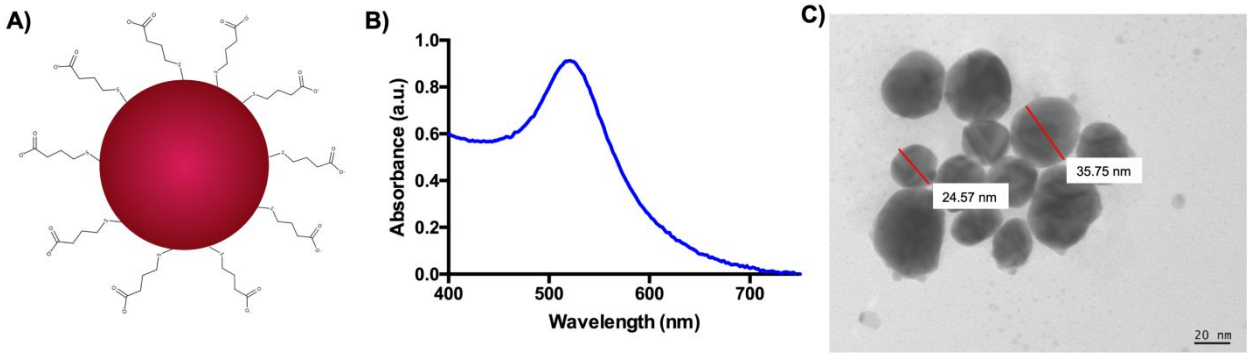

Figure 1. AuNP characterization. A) AuNPs-COOH chemical structure. B) UV/Vis reading showed an absorbance peak around 528 nm. C) The AuNPs-COOH present a rounded morphology with a diameter of ~32 nm, as shown via TEM analysis.

The RTG-lysine then had its free primary amine groups covalently conjugated to the AuNPs-COOH to obtain RTG-AuNPs, as shown in **Scheme 2**.

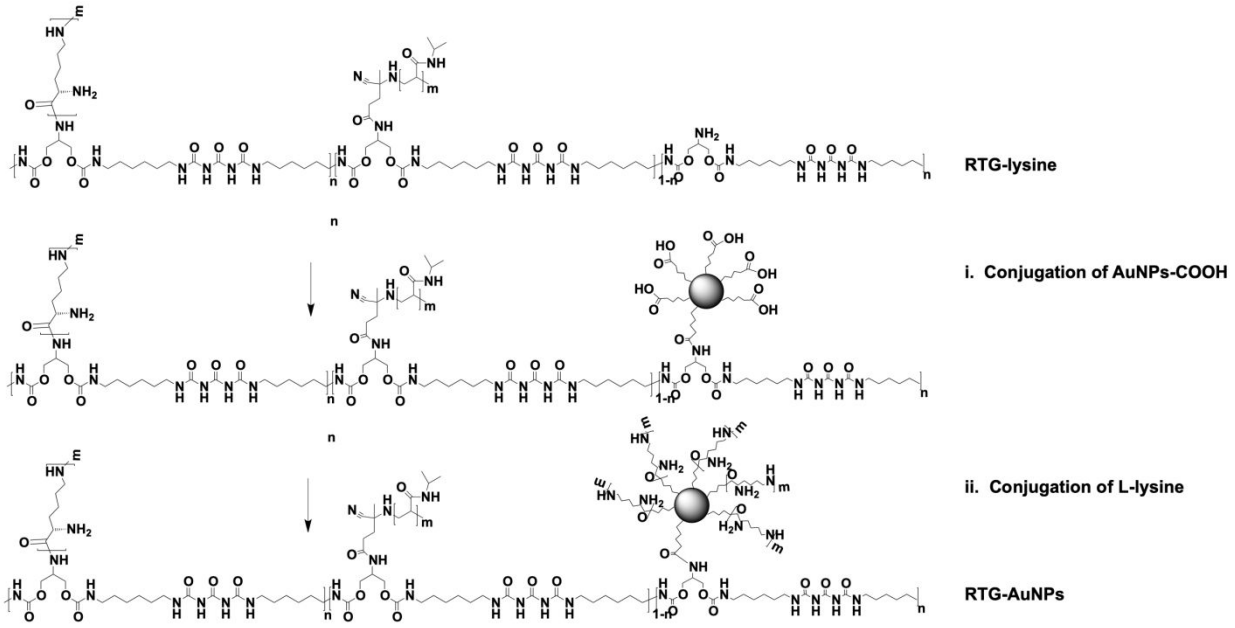

Scheme 2. Representation of the RTG-AuNPs synthesis.

To confirm the chemical linkage of the AuNPs within the RTG-lysine, TGA analysis was performed (**Figure 2A**). No component separation was observed during the material decomposition in both the RTG-lysine and RTG-AuNPs hydrogels, meaning no residuals of unreacted compounds[12]. The single weight loss in the RTG-AuNPs confirms the chemical conjugation of the AuNPs to the RTG-lysine backbone. Both polymer systems presented similar decomposition kinetics; initial decomposition of the RTG-lysine was observed at 435°C with a mass of 97%, while the RTG-AuNPs began to decompose at 425°C with a mass loss of 95%. Both

polymers were completely decomposed by 700°C. As expected, resistance of the RTG-AuNPs polymer was found to be significantly lower than that of the RTG-lysine (hydrogel without conjugated AuNPs), as measured at 37°C (140.1 KΩ ± 34.9 and 333.653 KΩ ± 50.46, respectively), validating the conductive properties of the RTG-AuNPs **(Figure 2B).**

The mechanical properties of both hydrogels were determined using oscillatory shear rheology (**Figure 2C**). Both hydrogels were found to have a sol-to-gel phase transition of approximately 35°C, making them ideal for biomedical applications as this is close to body temperature. Viscoelastic properties of both hydrogels were present at 37°C, however the RTG-AuNPs presented a significantly higher G' moduli (G' = 255.3 ± 45.2 Pa; n=6) than the RTG-lysine (G' = 181.7 ± 53.06 Pa; n=6) (**Figure S1B**). A frequency sweep analysis was also performed. **Figure S1C** shows that below 1 rad/sec the hydrogels present viscoelastic properties that increase with the angular frequency. At high frequencies, above 1 rad/sec, G" values dominate in both hydrogels.

The viscosities of both hydrogels were also analyzed. NRVM culture media was used for comparison. Both RTG-lysine and RTG-AuNPs solutions (at 3% [w/w]) possess viscosities similar to that of cell culture media (**Figure 2D**) (media: 21.9 ± 0.7 mPa.s; RTG-lysine: 22.58 ±1.3 mPa.s; RTG-AuNPs: 23.56 ± 2.5 mPa.s).

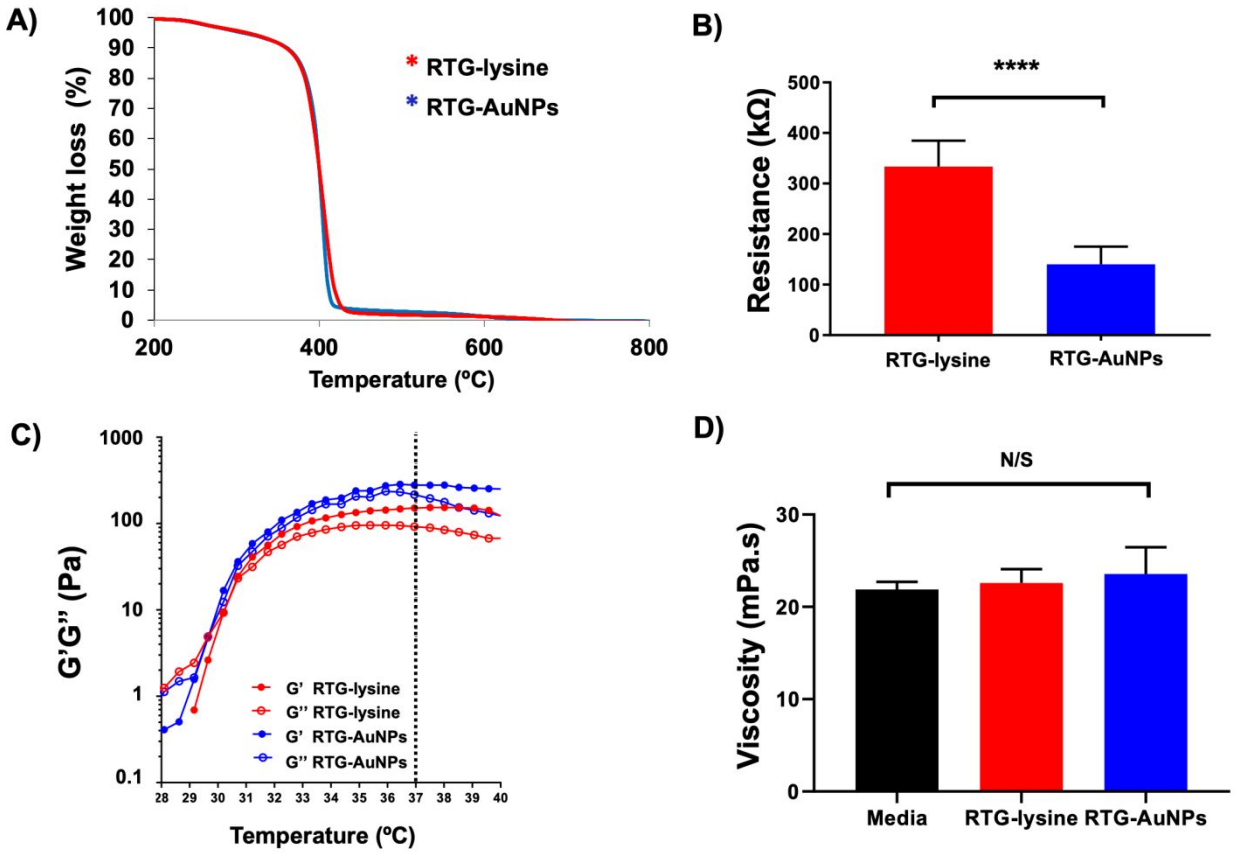

Figure 2. Characterization of the RTG-lysine and RTG-AuNPs hydrogels. A) a single weight loss monitored by TGA analysis demonstrates AuNPs chemical conjugation to the RTG-lysine. B) Resistance measurements demonstrating that the RTG-AuNPs system is more conductive than the RTG-lysine system. p value: ****<0.0001. Data are presented as mean ± S.D. C). The RTG-AuNPs system presents significantly higher mechanical properties to those of the RTG-lysine system. Data are presented as mean ± S.D. D) The viscosity of both the RTG-AuNPs and RTG-lysine systems at 3% (w/w) concentration are similar to that of the NRVM cell culture media. (N/S: non-significant). Data presented as mean ± S.D

XPS analysis was performed to further confirm the presence of the AuNPs in the RTG-AuNPs. **Figure 3A** shows XPS survey spectra of the RTG-AuNPs and the RTG-lysine hydrogels. As expected, the results demonstrate the presence of Au4f in the RTG-AuNPs hydrogel. Elemental analysis revealed that Au comprises around 0.3% of the hydrogel composition (**Figure 3B**).

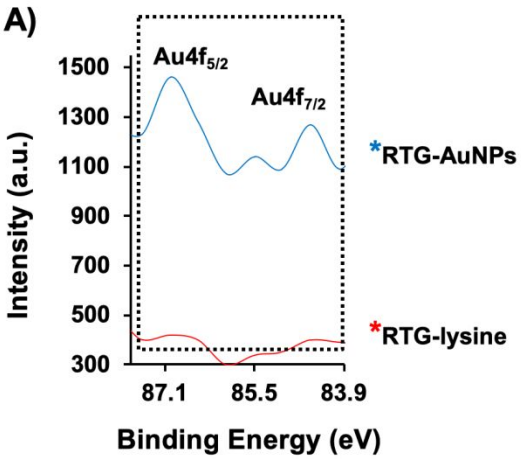

B)

	% Elemental Analysis			
	C	O	N	Au
RTG-AuNPs	57.59	31.69	10.52	0.28
RTG-Lysine	76.26	15.4	8.6	0

Figure 3. High-resolution XPS spectra relevant to Au4f regions of RTG-AuNP and RTG-lysine hydrogels, respectively. A) Characteristic peaks of Au4f were observed at 87 and 84.5 eV which confirm the presence of AuNPs in the RTG-AuNPs. B) Elemental analysis of both hydrogels further indicates the AuNPs within the RTG-AuNPs.

3D morphological characterization of the RTG-AuNPs system was also performed. Side and cross sections (generated via vertical and horizontal cuts, respectively, as shown in **Figure 4A**) revealed the 3D structure of the RTG-AuNPs system. Specifically, side sections demonstrated that the RTG-AuNPs assemble into a laminar sheet-like conformation upon gelling, providing a structure ideal for supporting cell orientation (**Figure 4B**). Cross sections revealed a highly interconnected and porous network (**Figure 4C**).

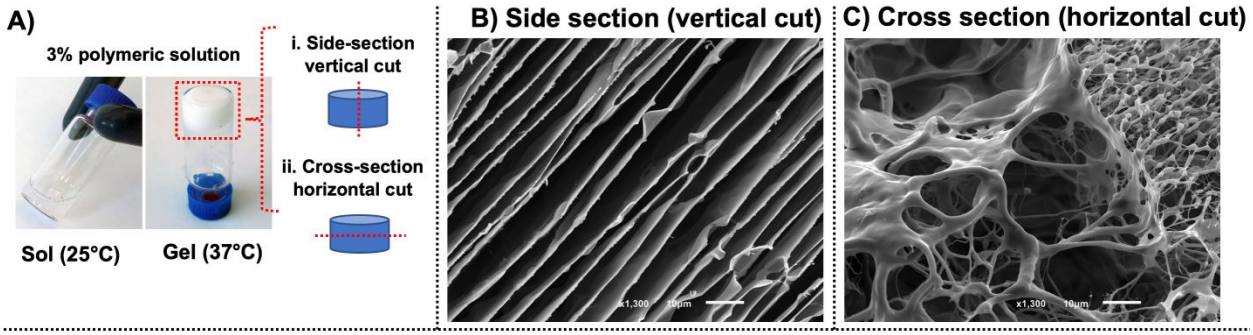

Figure 4. A) The morphological characterization of the RTG-AuNPs was analyzed in vertical and horizontal cuts. B) Vertical cuts of the hydrogel demonstrate a laminar sheet-like configuration. C) Horizontal cuts of the hydrogel showed a highly interconnected porosity.

***In vitro* long-term survival of NRVM and CF co-culture.** To determine whether the RTG-AuNPs hydrogel would be supportive of long-term 3D culture of cells similar to those found *in vivo*, we co-cultured NRVMs and CFs within this hydrogel system over a period of 21 days. CFs normally comprise approximately 10% of the total cell population derived from our standard NRVM preparation protocol[36,37]. We had previously analyzed the cell population of the non-cardiomyocyte cells within our cell culture isolation protocol and we were not able to detect non-cardiomyocyte cells but CFs only[28,34]. The RTG-lysine hydrogel and traditional 2D, gelatin-coated-dishes were both used as controls; such gelatin-coated dishes are typically recommended and used to successfully culture NRVM[35]. Both 2D and 3D culture systems received the same growth media, using a similar media change schedule protocol. Following 21 days of culture in the 3D or 2D systems, immunocytochemistry was performed using antibodies against α-actinin, a CM-specific marker, and vimentin, a CF-specific marker (**Figure 5A**), to determine how the percentages of subpopulations varied in these culture systems. Confocal microscopy revealed that

a significantly greater percentage of cells expressed α-actinin (i.e., were NRVMs) in the RTG-AuNPs system compared to the 2D gelatin control system (56% ± 10 vs. 43.3% ± 7.7, respectively). The percentage of α-actinin-positive cells was significantly higher in the RTG-lysine system (73.5% ± 0.97) compared to both the 2D gelatin control and RTG-AuNPs system (**Figure 5B**).

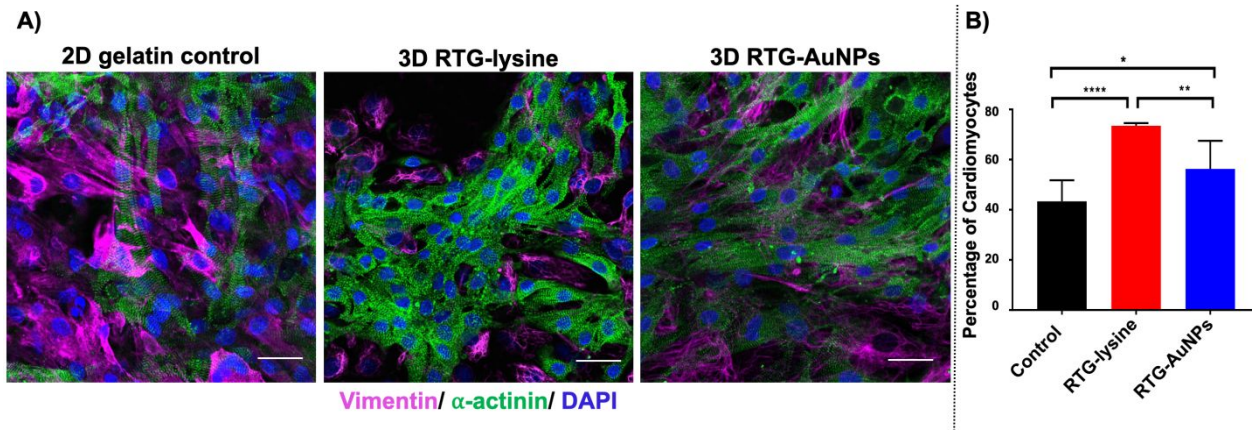

Figure 5. Immunocytochemistry labeling of NRVMs and CFs cultured in 2D and 3D systems for 21 days. A) Antibody staining against α-actinin (green) and vimentin (pink) label NRVMs and CFs, respectively, with nuclei labeled using DAPI (blue). B) Quantification of immunocytochemistry staining against α-actinin indicates percentage of cells likely to be NRVMs, showing both 3D systems to contain a greater percentage of NRVMs than the 2D gelatin control. Scale bar 40 μm. p values: *<0.023, **<0.0017 and ****<0.0001. Data are presented as mean ± S.D.

Following 21 days of culture in the 3D or 2D systems, immunocytochemistry was performed using an antibody against connexin 43 (Cx43), a gap junction protein, to determine the degree and localization of expression of this protein in the culture systems (**Figure 6A**). Confocal microscopy

revealed cells cultured in the RTG-AuNPs hydrogel have stet greater Cx43 staining area (3.2 ± 1.96 μm^2) compared to cells in the 2D gelatin control system (0.26 ± 0.1 μm^2) and the RTG-lysine system (0.89 ± 0.13 μm^2) (**Figure 6B**).

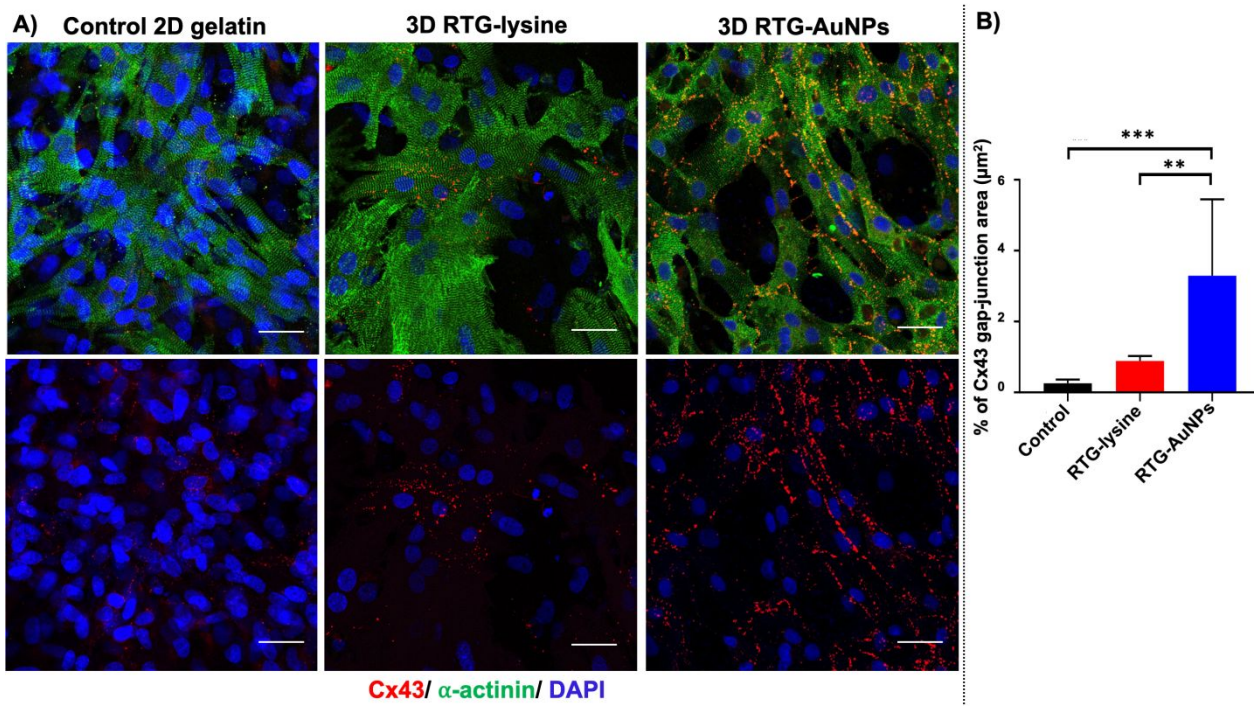

Figure 6. Immunocytochemistry labeling of gap junctions in NRVMs cultured in 2D and 3D systems for 21 days. (A) Antibody staining against connexin 43 (Cx43) (red) and α-actinin (green), with nuclei labeled using DAPI (blue). (B) Quantification of immunocytochemistry staining against Cx43 to indicate surface area of NRVMs positive for this gap junction protein, showing the RTG-AuNPs system to contain the largest Cx43-positive area. Scale bar: 40 μm. p values: **<0.0021 and *** <0.0002. Data are presented as mean ± S.D.

Discussion. Previously we demonstrated that our RTG-lysine hydrogel system supports long-term cardiomyocyte survival for up to 21 days. For the current work, our aim was to develop a conductive, injectable RTG functionalized with AuNPs and to assess its ability to function as a 3D

scaffold supportive of a co-culture of CMs and CFs but emphasizing long-term CMs survival. AuNPs were selected as an ideal conductive material to incorporate due to their high biocompatibility and inert properties[27,38]. In addition, several recent studies have shown that polymeric materials functionalized with AuNPs can improve electrical communication between conductive cells such as CMs and neurons[39]. For example, Nair et al. found that a decellularized porcine matrix conjugated with AuNPs promoted growth and proliferation of rat myoblasts (H9C2 cells) [40]. Similarly, Shevach et al. found that fibrous decellularized omental matrices with deposited AuNPs improved elongation, alignment, and cardiac function of NRVMs (compared to matrices devoid of AuNPs) [22]. Baranes et al. similarly demonstrated that AuNPs embedded within the surface of electrospun nanofibers encouraged longer neurite outgrowth of primary neurons[23].

In this work, we were able to chemically incorporate AuNPs-COOH within our highly biocompatible RTG-lysine hydrogel. AuNPs-COOH were characterized with TEM and UV/Vis spectroscopy. It has been reported that spherical AuNPs diameter can be calculated using multipole scattering theory from UV/Vis spectroscopy data[41,42]. Using this method, we determined the diameter of the AuNPs-COOH, which was in the range of 35 nm. Similar values were obtained using TEM (32 +/- 8 nm), demonstrating the precision of this approach. AuNPs-COOH were well dispersed in water as shown in **Figure S1A**. This property simplified their conjugation within the RTG-lysine hydrogel and avoided the use of further polymer purification methods. The chemical incorporation of AuNPs-COOH was demonstrated by both TGA and XPS. TGA results show a single weight loss event in the RTG-AuNPs hydrogel, meaning no residuals of unreacted compounds[34]. These results confirm the conjugation of the AuNPs to the RTG-lysine backbone. The presence of gold and its % composition within the polymer was evaluated by XPS. **Figure 3** shows a high resolution XPS spectra of the RTG-lysine and the RTG-AuNPs in which two doublets

of Au 4f, Au 4f $_{5/7}$ and Au 4f $_{7/2}$, located at 87.1 and 84. 5 eV are present in the RTG-AuNPs hydrogel. The positions of these doublets are similar to those reported by other authors[43–45], thus demonstrating that the AuNPs were well conjugated into the RTG-lysine hydrogel.

The injectable RTG-AuNPs hydrogel system presented here holds several advantages over bioengineered patch systems. The first advantage of the RTG-AuNPs system is that it possesses a highly porous structure that is able to host embedded cells within its 3D matrix. Thanks to its highly interconnected porosity, encapsulated cells can easily elongate and interconnect with each other, without forced rearrangement of their surrounding microenvironment. It has previously been reported that the porosity and pore size of 3D scaffolds unsurprisingly has an important effect on encapsulated cells, as open and interconnected porous networks are essential for proper cell nutrition, proliferation, and migration[46,47]. As previously mentioned, side sections of the RTG-AuNPs observed via SEM show a laminar sheet-like configuration, which likely aids in proper NRVM orientation and elongation. Cell alignment is particularly important for immature CMs as it promotes mechanical integrity, electrical conduction, contractile efficiency and ultimately leads to cell maturation[48–51]. A laminar sheet-like configuration has been also observed in our other RTG systems as well[30] and it has favored other cell types. We have previously reported that this laminar assembly depends on the concentration of the polymer solution[30]. Hydrogels with polymer concentrations belong 2.5 %, (W/W %) assemble into heterogeneous structures[30].

A second advantage of the RTG-AuNPs system is that it possesses decreased resistance, and thus increased conductivity, compared to the RTG-lysine system. Although the resistance of metallic bulk gold is in approximately 2.4 x 10^{-11} KΩ[52,53], a reflection of it being it a highly conductive material, the number of free amine groups in the RTG-lysine system limits the number of AuNPs-COOH conjugation sites and thus, the amount of Au within the RTG-AuNPs was only

0.3% as estimated by XPS elemental analysis. However, despite the small amount of AuNPs conjugated with the RTG-lysine hydrogel, the RTG-AuNPs hydrogel still has a higher resistance than the plain RTG-lysine and that can be appreciated in the increased amount of Cx43 observed within the CMs cultured in the RTG-AuNPs hydrogel.

Another advantage of the RTG-AuNPs hydrogel is its low viscosity, which is similar to that of cell culture media. This property allows the RTG-lysine and the RTG-AuNPs hydrogels to be easily injected through a small gauge needle, as demonstrated in the supportive information videos S1 and S2. It has been previously reported that hydrogels with low viscosity are easier to inject than hydrogels with a high viscosity [54]. From an application point of view, minimally invasive therapies are very appealing for tissue engineering approaches[12,55] and therefore the injectable property of RTG-AuNPs is a major advantage for both *in vivo* studies and future translational therapeutic applications.

In the current work, we aimed to first develop and characterize the injectable biocompatible conductive hydrogel. We were able to show that both the mechanical properties, storage and loss modulus of the RTG-AuNPs hydrogel are low, which is characteristic of physical gels at low polymer concentration[28,34]. Moreover, we found that at high angular frequency (above 1 rad/sec) both hydrogels behave like viscoelastic liquids. These results further confirm that both RTG hydrogels are weak gels due to their weak physical gelation properties[56]. Although we have reported previously that increasing the concentration of the polymer in solution leads to an increase in the mechanical properties of the type of RTG hydrogels tested for this investigation[30], several investigations have reported the successful use of hydrogels with low mechanical properties in both *in vitro*[28,34,57–60] and in *in vivo*[61,62] cardiac tissue engineering studies. We have previously demonstrated that NRVMs cultured in our soft 3D RTG-lysine hydrogel present long-term

viability for up to 21 days with increased Cx43 area when compared with traditional 2D gelatin controls[28]. We also demonstrate the functional improvement of NRVMs cultured in 3D RTG-CNT soft gels and their increased Cx43 area and more homogeneous calcium transients for up to 21 days when cultured in these soft hydrogels systems[34]. Geuss et al. demonstrated that HL-1 cardiomyocytes cultured in PEGylated Fibrin hydrogels, with storage moduli of 123.5 $\pm$ 29.6 Pa, spread better than PEGylated Fibrin hydrogels, with storage moduli of 966.8 + 85.5 Pa[59]. Hao et al. tested fulleren/alginate hydrogels, with storage moduli in the range of 600 Pa, as a delivery system of brown adipose-derived stem cells in a rat MI model. They demonstrated that the hydrogels improve the retention and survival of the implanted cells and induced angiogenesis, which promoted cardiac function recovery[61]. Singelyn et al. proved that hydrogels derived from decellularized pig ventricular extracellular matrix, with low mechanical properties, were able to maintain cardiac function in a rat MI model without inducing arrhythmias[63]. Wassennaar et al. have shown that porcine myocardial hydrogel with low mechanical properties alters several remodeling pathways after MI promoting pro-regenerative environment in the injured tissue[64]. Moreover, Rane et al. has demonstrated that structural reinforcement of injured cardiac tissue, due to the mechanical properties of hydrogels, is insufficient to prevent cardiac remodeling: they found that bioactivity and cell infiltration within injectable materials have a key role in improving cardiac function in the injured tissue[65].

Material degradation is another important property for tissue engineering applications. While degradable hydrogels may be desirable, inert, non-degradable materials can also be used for cardiac regeneration[11]. We have previously reported that modifying the chemistry composition of the PNIPAAm co-polymer used in the synthesis of our RTG systems can lead to fast or slow degradations rates of our hydrogels[66].

Finally, we evaluated the ability of our RTG-AuNPs system to support NRVMs and CF in a co-culture. This analysis was crucial to determine the feasibility of this material for use as a scaffold in cardiac tissue applications. As discussed above, we encapsulated a co-culture of NRVMs and CFs within the RTG-AuNPs system. Because the RTG-AuNPs is in a solution at room temperature, encapsulation of cardiac cells was easily achieved through simple mixing of the RTG-AuNPs with the cell suspension at room temperature. While the electroactive RTG-AuNPs maintained the growth of NRVMs in co-culture with CFs for at least 21 days, the percentage of NRVMs was surprisingly lower in the 3D RTG-AuNPs system compared with the RTG-lysine system. However, this may be beneficial for the NRVMs as CFs provide mechanotransductive cues that can improve CM function[67]. Finally, we demonstrated that when cultured in the 3D RTG-AuNPs, the NRVMs had a significantly greater area of Cx43-positive cells when compared to 2D gelatin controls and the RTG-lysine hydrogel. This may be due to the electrical cues of the RTG-AuNPs promoting a more organized, and hence better defined, area of Cx43 expression. It has been reported by several authors that correct organization of Cx43 plays an important role for normal cardiac function. Unorganized Cx43 can lead to cardiac arrhythmias[68–70]. Here we have demonstrated that RTG-AuNPs hydrogel induces a more organized and increased Cx43 localization, which is beneficial for CM function[36]. Overall, our results suggest that the RTG-AuNPs system supports long-term cardiac cell survival (for at least 21 days) in co-culture with CFs with increased and more organized Cx43 expression, making the RTG-AuNPs polymer promising for use in *in vivo* applications (on-going study). Although this study was performed with cardiac cells, this system should not be limited for cardiac tissue engineering applications as it can be beneficial for other conductive cells such as neurons.

Conclusion. Here we demonstrate that our injectable, conductive, and low viscosity RTG-AuNP hydrogel, which conveniently transitions to a 3D matrix by temperature stimuli, can provide both topographical and electrophysiological cues supportive of culturing both NRVMs and CFs. This system specifically promotes long-term CM survival with an increased surface area positive for Cx43. Finally, we believe that our RTG-AuNPs system holds tremendous potential for both minimally invasive approaches to repairing damaged heart tissues as well as use for 3D *in vitro* cardiac modeling investigations.

ASSOCIATED CONTENT

Supporting Information.

The Supporting Information is available free of charge on the ACS Publications website.

AUTHOR INFORMATION

***Corresponding authors:**

Daewon Park: Department of Bioengineering, University of Colorado Denver Anschutz Medical Campus, 12800 E. 19th Avenue, Aurora CO 80045, Tel. 303-724-6947, Email: daewon.park@ucdenver.edu.

Luisa Mestroni: Cardiovascular Institute, University of Colorado Denver Anschutz Medical Campus, 12700 E. 19th Avenue, Aurora CO 80045, Tel. 303-724-0858, Email: luisa.mestroni@ucdenver.edu.

Present Addresses

[1] Department of Medicine, Division of Cardiology, University of Colorado Anschutz Medical Campus, at 12700 E.19th Avenue, Bldg. P15, Aurora, Colorado, 80045, United States.

[2] Bioengineering Department, University of Colorado Denver Anschutz Medical Campus, at Bioscience 2 1270 E. Montview Avenue, Suite 100, Aurora, Colorado, 80045, United States.

[3]Department of Chemistry, Metropolitan State University of Denver, at 1201 5th St, Denver, Colorado, 80206, United States.

[4] Department of Chemical and Biological Engineering and the BioFrontiers Institute, University of Colorado at Boulder, 3415 Colorado Avenue, Boulder, Colorado, 80309, United States.

[5] Carbon Nanobiotechnology Laboratory CIC biomaGUNE, Paseo de Miramón 182 20009 Donostia-San Sebastián, 20009, Spain.

[6] POLYMAT, University of the Basque Country UPV/EHU, Avenida de Tolosa 72, 20018 Donostia-San Sebastián, Spain.

[7] Department of Chemical and Pharmaceutical Sciences, University of Trieste, Via Giorgieri 1, Trieste, 34127, Italy.

[8] Basque Fdn Sci, Ikerbasque, Bilbao 48013, Spain.

[9] Consortium for Fibrosis Research & Translation, University of Colorado Anschutz Medical Campus, Aurora, CO 80045, United States.

†TR address is different than the one given in the affiliation line: Current address for TR is Department of Biochemistry and BioFrontiers Institute, U. of Colorado Boulder, Boulder, CO 80309.

Author Contributions

The manuscript was written through contributions of all authors. All authors have given approval to the final version of the manuscript. BP performed all the polymer synthesis experiments, SEM characterization, viscosity analysis, cell isolation, *in vitro* cell studies, cell staining, and cell imaging. MM and AB carried out the AuNPs synthesis and characterization. BA characterized the mechanical properties of the hydrogels. NLF helped to analyze the resistance propertied of the materials. AD performed the TGA analysis.

Funding Sources

This study was supported by generous grants of the John Patrick Albright (LM, MT and BP) and Foreman Casali (LM) Foundations, NIH/NHLBI RO1 HL116905 (LM), NIH (HL116848 and HL127240) (T.A.M), American Heart Association (16SFRN31400013) (T.A.M), PDS HL116906 (BP), AHA SFRN Heart Failure Fellow (16SFRN31400013) (BP), 1RO1HL109209-01A1 (MT), NIH RO1 HL114753 (RS), NIH K24 HL081506 (RS), NIH F32 (1 F32 HL137256-01) (BA) and the Burroughs Welcome Fund Postdoctoral Enrichment Program (BA). This work was supported in part by a Trans-Atlantic Network of Excellence grant from the Leducq Foundation (14 CVD 03) (LM, MT and BP). Part of this work was supported by AXA research funds (MP), the Spanish Ministry of Economy and Competitiveness MINECO (project CTQ2016-76721-R) (MP), the

University of Trieste and the Maria de Maeztu Units of Excellence Program from the Spanish State Research Agency – Grant No. MDM-2017-0720 (MP). This investigation was also supported in part by the AHA (17GRNT33661024) (DP) and the R21 HL124100-01 (DP).

ACKNOWLEDGMENT

The authors would like to thank Walther R. Olivas for helping with the injection videos. The authors would like also to thank the University of Colorado Denver Advanced Microscopy Core for their facilities and support. The authors also thank Eric P. Wartchow and the Electron Microscopy Lab at Children's Hospital Colorado for facilities and support in the SEM and TEM analysis. Dr. Pena would like to specially thank Dr. Peter Buttrick for all his help, support and advise during this investigation.

ABBREVIATIONS

RTG: Reverse Thermal Gel, AuNPs: gold nanoparticles, 3D: three dimensional, NRVM: Neonatal Rat Ventricular Myocytes, TGA: Thermo Gravimetric Analysis, SEM: scanning electron Microscopy, XPS: X-ray photoelectron spectroscopy, CMs: cardiomyocytes, CFs: cardiac fibroblast.

REFERENCES

(1) Konstam, M. A.; Kramer, D. G.; Patel, A. R.; Maron, M. S.; Udelson, J. E. Left Ventricular Remodeling in Heart Failure: Current Concepts in Clinical Significance and Assessment. *JACC Cardiovasc. Imaging* **2011**, *4* (1), 98–108.

(2) Inamdar, A.; Inamdar, A. Heart Failure: Diagnosis, Management and Utilization. *J. Clin. Med.* **2016**, *5* (7), 62.

(3) Cho, E.; Kim, M.; Ko, Y. S.; Lee, H. Y.; Song, M.; Kim, M. G.; Kim, H. K.; Cho, W. Y.; Jo, S. K. Role of Inflammation in the Pathogenesis of Cardiorenal Syndrome in a Rat Myocardial Infarction Model. *Nephrol. Dial. Transplant.* **2013**, *28* (11), 2766–2778.

(4) Braunwald, E. Heart Failure. *JACC Hear. Fail.* **2013**, *1* (1), 1–20.

(5) Li, S.; Loganathan, S.; Korkmaz, S.; Radovits, T.; Hegedus, P.; Zhou, Y.; Karck, M.; Szabó, G. Transplantation of Donor Hearts after Circulatory or Brain Death in a Rat Model. *J. Surg. Res.* **2015**, *195* (1), 315–324.

(6) Barr, M. L.; Taylor, D. O. Changes in Donor Heart Allocation in the United States without Fundamental Changes in the System: Rearranging Deck Chairs and Elephants in the Room. *Am. J. Transplant.* **2015**, *15* (1), 7–9.

(7) Chin, C.; Miller, J.; Robbins, R.; Reitz, B.; Bernstein, D. The Use of Advanced-Age Donor Hearts Adversely Affects Survival in Pediatric Heart Transplantation. *Pediatr Transpl.* **1999**, *3* (4), 309–314.

(8) Nelson, D. M.; Ma, Z.; Fujimoto, K. L.; Hashizume, R.; Wagner, W. R. Intra-Myocardial Biomaterial Injection Therapy in the Treatment of Heart Failure: Materials, Outcomes and Challenges. *Acta Biomater.* **2011**, *7* (1), 1–15.

(9) Johnson, T. D.; Braden, R. L.; Christman, K. L. Cardiac Tissue Engineering. **2014**, *1181* (6), 109–120.

(10) Tous, E.; Purcell, B.; Ifkovits, J. L.; Burdick, J. A. Injectable Acellular Hydrogels for Cardiac Repair. *J. Cardiovasc. Transl. Res.* **2011**, *4* (5), 528–542.

(11) Radisic, M.; Christman, K. L. Materials Science and Tissue Engineering: Repairing the

Heart. *Mayo Clin. Proc.* **2013**, *88* (8), 884–898.

(12) Peña, B.; Laughter, M.; Jett, S.; Rowland, T. J.; Taylor, M. R. G.; Mestroni, L.; Park, D. Injectable Hydrogels for Cardiac Tissue Engineering. *Macromol. Biosci.* **2018**, *18* (6), 1–22.

(13) Hasan, A.; Khattab, A.; Islam, M. A.; Hweij, K. A.; Zeitouny, J.; Waters, R.; Sayegh, M.; Hossain, M. M.; Paul, A. Injectable Hydrogels for Cardiac Tissue Repair after Myocardial Infarction. *Adv. Sci.* **2015**, *2* (11), 1–18.

(14) Janani, A.; Sridhar Skylab, R. Injectable Hydrogel for Cardiac Tissue Engineering. *Int. J. ChemTech Res.* **2014**, *6* (3), 2233–2236.

(15) Aguado, B. A.; Mulyasasmita, W.; Su, J.; Ph, D.; Lampe, K. J.; Ph, D.; Heilshorn, S. C.; Ph, D. Improving Viability of Stem Cells During Syringe Needle Flow Through the Design of Hydrogel Cell Carriers. *Tissue Eng. Part A* **2012**, *18* (7–8), 806–815.

(16) Hirt, M. N.; Hansen, A.; Eschenhagen, T. Cardiac Tissue Engineering : State of the Art. *Circ. Res.* **2014**, *114* (2), 354–367.

(17) Park, M. H.; Joo, M. K.; Choi, B. G.; Jeong, B. Biodegradable Thermogels. *Acc. Chem. Res.* **2012**, *45* (3), 424–433.

(18) Rastogi, R. P.; Richa; Kumar, A.; Tyagi, M. B.; Sinha, R. P. Molecular Mechanisms of Ultraviolet Radiation-Induced DNA Damage and Repair. *J. Nucleic Acids* **2010**, *2010*, 1–32.

(19) Tandon, N.; Cannizzaro, C.; Chao, P.-H. G.; Maidhof, R.; Marsano, A.; Au, H. T. H.; Radisic, M.; Vunjak-Novakovic, G. Electrical Stimulation Systems for Cardiac Tissue Engineering. *Nat. Protoc.* **2009**, *4* (2), 155–173.

(20) Shin, S. R.; Jung, S. M.; Zalabany, M.; Kim, K.; Zorlutuna, P.; Kim, S. B.; Nikkhah, M.;

Khabiry, M.; Azize, M.; Kong, J.; Wan, K. T.; Palacios, T.; Dokmeci, M. R.; Bae, H.; Tang, X.; Khademhosseini, A. Carbon-Nanotube-Embedded Hydrogel Sheets for Engineering Cardiac Constructs and Bioactuators. *ACS Nano* **2013**, *7* (3), 2369–2380.

(21) Li, Y.; Shi, X.; Tian, L.; Sun, H.; Wu, Y.; Li, X.; Li, J.; Wei, Y.; Han, X.; Zhang, J.; Jia, X.; Bai, R.; Jing, L.; Ding, P.; Liu, H.; Han, D. AuNP–Collagen Matrix with Localized Stiffness for Cardiac-Tissue Engineering: Enhancing the Assembly of Intercalated Discs by B1-Integrin-Mediated Signaling. *Adv. Mater.* **2016**, *28* (46), 10230–10235.

(22) Shevach, M.; Fleischer, S.; Shapira, A.; Dvir, T. Gold Nanoparticle-Decellularized Matrix Hybrids for Cardiac Tissue Engineering. *Nano Lett.* **2014**, *14* (10), 5792–5796.

(23) Baranes, K.; Shevach, M.; Shefi, O.; Dvir, T. Gold Nanoparticle-Decorated Scaffolds Promote Neuronal Differentiation and Maturation. *Nano Lett.* **2016**, *16* (5), 2916–2920.

(24) McCaffrey, R.; Long, H.; Jin, Y.; Sanders, A.; Park, W.; Zhang, W. Template Synthesis of Gold Nanoparticles with an Organic Molecular Cage. *J. Am. Chem. Soc.* **2014**, *136* (5), 1782–1785.

(25) Wu, Y.; Li, Y.; Liu, P.; Gardner, S.; Ong, B. S. Studies of Gold Nanoparticles as Precursors to Printed Conductive Features for Thin-Film Transistors. *Chem. Mater.* **2006**, *18* (19), 4627–4632.

(26) He, L.; Dragavon, J.; Cho, S.; Mao, C.; Yildirim, A.; Ma, K.; Chattaraj, R.; Goodwin, A. P.; Park, W.; Cha, J. N. Self-Assembled Gold Nanostar-NaYF4:Yb/Er Clusters for Multimodal Imaging, Photothermal and Photodynamic Therapy. *J. Mater. Chem. B* **2016**, *4* (25), 4455–4461.

(27) Martín, C.; Merino, S.; Prato, M.; Vázquez, E.; Kostarelos, K. Nanocomposite Hydrogels: 3D Polymer–Nanoparticle Synergies for On-Demand Drug Delivery. *ACS Nano* **2015**, *9*

(5), 4686–4697.

(28) Peña, B.; Martinelli, V.; Jeong, M.; Bosi, S.; Lapasin, R.; Taylor, M. R. G. G.; Long, C. S.; Shandas, R.; Park, D.; Mestroni, L. Biomimetic Polymers for Cardiac Tissue Engineering. *Biomacromolecules* **2016**, *17* (5), 1593–1601.

(29) Peña, B.; Shandas, R.; Park, D. A Heparin-Mimicking Reverse Thermal Gel for Controlled Delivery of Positively Charged Proteins. *J. Biomed. Mater. Res. - Part A* **2015**, *103* (6), 2102–2108.

(30) Laughter, M. R.; Ammar, D. A.; Bardill, J. R.; Pena, B.; Kahook, M. Y.; Lee, D. J.; Park, D. A Self-Assembling Injectable Biomimetic Microenvironment Encourages Retinal Ganglion Cell Axon Extension in Vitro. *ACS Appl. Mater. Interfaces* **2016**, *8* (32), 20540–20548.

(31) Yun, D.; Famili, A.; Lee, Y. M.; Jenkins, P. M.; Freed, C. R.; Park, D. Biomimetic Poly(Serinol Hexamethylene Urea) for Promotion of Neurite Outgrowth and Guidance. *J. Biomater. Sci. Polym. Ed.* **2014**, *25* (March), 354–369.

(32) Yun, D.; Laughter, M. R.; Park, D. A Biomimetic Reverse Thermal Gel for 3-Dimensional Neural Tissue Engineering. *Austin J. Biomed. Eng.* **2014**, *1* (4), 1–5.

(33) Jenkins, P. M.; Laughter, M. R.; Lee, D. J.; Lee, Y. M.; Freed, C. R.; Park, D. A Nerve Guidance Conduit with Topographical and Biochemical Cues: Potential Application Using Human Neural Stem Cells. *Nanoscale Res. Lett.* **2015**, *10* (1), 972.

(34) Peña, B.; Bosi, S.; Aguado, B. A.; Borin, D.; Farnsworth, N. L.; Dobrinskikh, E.; Rowland, T. J.; Martinelli, V.; Jeong, M.; Taylor, M. R. G. G.; Long, C. S.; Shandas, R.; Sbaizero, O.; Prato, M.; Anseth, K. S.; Park, D.; Mestroni, L. Injectable Carbon Nanotube-Functionalized Reverse Thermal Gel Promotes Cardiomyocytes Survival and Maturation.

ACS Appl. Mater. Interfaces **2017**, *9* (37), 31645–31656.

(35) Martinelli, V.; Cellot, G.; Toma, F. M.; Long, C. S.; Caldwell, J. H.; Zentilin, L.; Giacca, M.; Turco, A.; Prato, M.; Ballerini, L.; Mestroni, L. Carbon Nanotubes Promote Growth and Spontaneous Electrical Activity in Cultured Cardiac Myocytes. *Nano Lett.* **2012**, *12* (4), 1831–1838.

(36) Martinelli, V.; Cellot, G.; Toma, F. M.; Long, C. S.; Caldwell, J. H.; Zentilin, L.; Giacca, M.; Turco, A.; Prato, M.; Ballerini, L.; Mestroni, L. Carbon Nanotubes Instruct Physiological Growth and Functionally Mature Syncytia: Nongenetic Engineering of Cardiac Myocytes. *ACS Nano* **2013**, *7* (7), 5746–5756.

(37) Martinelli, V.; Cellot, G.; Fabbro, A.; Bosi, S.; Mestroni, L.; Ballerini, L. Improving Cardiac Myocytes Performance by Carbon Nanotubes Platforms. *Front. Physiol.* **2013**, *4 SEP* (September), 1–6.

(38) Amezcua, R.; Shirolkar, A.; Fraze, C.; Stout, D. Nanomaterials for Cardiac Myocyte Tissue Engineering. *Nanomaterials* **2016**, *6* (7), 133.

(39) Vial, S.; Reis, R. L.; Oliveira, J. M. Recent Advances Using Gold Nanoparticles as a Promising Multimodal Tool for Tissue Engineering and Regenerative Medicine. *Curr. Opin. Solid State Mater. Sci.* **2017**, *21* (2), 92–112.

(40) Nair, R. S.; Ameer, J. M.; Alison, M. R.; Anilkumar, T. V. A Gold Nanoparticle Coated Porcine Cholecyst-Derived Bioscaffold for Cardiac Tissue Engineering. *Colloids Surfaces B Biointerfaces* **2017**, *157*, 130–137.

(41) Wolfgang Haiss, Nguyen T. K. Thanh, Jenny Aveyard, and D. G. F. Determination of Size and Concentration of Gold Nanoparticles from Extinction Spectra. *Anal. Chem.* **2007**, *79*, 4215–4221.

(42) Amendola, V.; Meneghetti, M. Size Evaluation of Gold Nanoparticles by UV # Vis Spectroscopy Size Evaluation of Gold Nanoparticles by UV - Vis Spectroscopy. *J. Phys. Chemestry C* **2009**, *113*, 4277–4285.

(43) Božanić, D. K.; Luyt, A. S.; Trandafilović, L. V.; Djoković, V. Glycogen and Gold Nanoparticle Bioconjugates: Controlled Plasmon Resonance via Glycogen-Induced Nanoparticle Aggregation. *RSC Adv.* **2013**, *3* (23), 8705–8713.

(44) Castillo, C.; Buono-Core, G.; Manzur, C.; Yutronic, N.; Sierpe, R.; Cabello, G.; Chornik, B. Molybdenum Trioxide Thin Films Doped with Gold Nanoparticles Grown by a Sequential Methodology: Photochemical Metal-Organic Deposition (PMOD) and DC-Magnetron Sputtering. *J. Chil. Chem. Soc.* **2016**, *61* (1), 2816–2820.

(45) Ke, X.; Zhang, X.; Zhao, J.; Sarina, S.; Barry, J.; Zhu, H. Selective Reductions Using Visible Light Photocatalysts of Supported Gold Nanoparticles. *Green Chem.* **2013**, *15* (1), 236–244.

(46) Annabi, N.; Nichol, J. W.; Zhong, X.; Ji, C.; Koshy, S.; Khademhosseini, A.; Dehghani, F. Controlling the Porosity and Microarchitecture of Hydrogels for Tissue Engineering. *Tissue Eng. Part B Rev.* **2010**, *16* (4), 371–383.

(47) Loh, Q. L.; Choong, C. Three-Dimensional Scaffolds for Tissue Engineering Applications: Role of Porosity and Pore Size. *Tissue Eng. Part B Rev.* **2013**, *19* (6), 485–502.

(48) Pasqualini, F. S.; Sheehy, S. P.; Agarwal, A.; Aratyn-Schaus, Y.; Parker, K. K. Structural Phenotyping of Stem Cell-Derived Cardiomyocytes. *Stem Cell Reports* **2015**, *4* (3), 340–347.

(49) Ye, F.; Keller, B. B.; Nakane, T.; Dwenger, M.; Yuan, F.; Masumoto, H.; Tinney, J. P.;

Kowalski, W. J. Quantification of Cardiomyocyte Alignment from Three-Dimensional (3D) Confocal Microscopy of Engineered Tissue. *Microsc. Microanal.* **2017**, *23* (04), 826–842.

(50) Weeke-Klimp, A.; Bax, N. A. M.; Bellu, A. R.; Winter, E. M.; Vrolijk, J.; Plantinga, J.; Maas, S.; Brinker, M.; Mahtab, E. A. F.; Gittenberger-de Groot, A. C.; van Luyn, M. J. A.; Harmsen, M. C.; Lie-Venema, H. Epicardium-Derived Cells Enhance Proliferation, Cellular Maturation and Alignment of Cardiomyocytes. *J. Mol. Cell. Cardiol.* **2010**, *49* (4), 606–616.

(51) Yajima, S.; Morone, N.; Wang, L.; Shiozaki, M.; Yu, L.; Liu, L.; Nakatsuji, N.; Yoshioka, M.; Li, J.; Li, S.; Qiao, J.; Fukushima, S.; Li, X.; Shiba, Y.; Sawa, Y.; Kotera, H.; Minami, I.; Miyagawa, S.; Chen, Y. Human Pluripotent Stem Cell-Derived Cardiac Tissue-like Constructs for Repairing the Infarcted Myocardium. *Stem Cell Reports* **2017**, *9* (5), 1546–1559.

(52) Lloyd David H. *Physics*, 2nd ed.; Saunders college Publishing: Florida, 1998.

(53) Cutnell, John D; Johnson, K. W. *Physics*, 4th ed.; Wiley: New York, 1998.

(54) Chen, M. H.; Wang, L. L.; Chung, J. J.; Kim, Y. H.; Atluri, P.; Burdick, J. A. Methods to Assess Shear-Thinning Hydrogels for Application As Injectable Biomaterials. *ACS Biomater. Sci. Eng.* **2017**, *3* (12), 3146–3160.

(55) Kondiah, P. J.; Choonara, Y. E.; Kondiah, P. P. D.; Marimuthu, T.; Kumar, P.; Du Toit, L. C.; Pillay, V. A Review of Injectable Polymeric Hydrogel Systems for Application in Bone Tissue Engineering. *Molecules* **2016**, *21* (11).

(56) Jyoti, B. V. S.; Baek, S. W. Rheological Characterization of Ethanolamine Gel Propellants. *J. Energ. Mater.* **2016**, *34* (3), 260–278.

(57) Jeffords, M. E.; Wu, J.; Shah, M.; Hong, Y.; Zhang, G. Tailoring Material Properties of Cardiac Matrix Hydrogels to Induce Endothelial Differentiation of Human Mesenchymal Stem Cells. *ACS Appl. Mater. Interfaces* **2015**, *7* (20), 11053–11061.

(58) Ungerleider, J. L.; Johnson, T. D.; Rao, N.; Christman, K. L. Fabrication and Characterization of Injectable Hydrogels Derived from Decellularized Skeletal and Cardiac Muscle. *Methods* **2015**, *84*, 53–59.

(59) Geuss, L. R.; Allen, A. C. B.; Ramamoorthy, D.; Suggs, L. J. Maintenance of HL-1 Cardiomyocyte Functional Activity in PEGylated Fibrin Gels. *Biotechnol. Bioeng.* **2015**, *112* (7), 1446–1456.

(60) Navaei, A.; Truong, D.; Heffernan, J.; Cutts, J.; Brafman, D.; Sirianni, R. W.; Vernon, B.; Nikkhah, M. PNIPAAm-Based Biohybrid Injectable Hydrogel for Cardiac Tissue Engineering. *Acta Biomater.* **2016**, *32*, 10–23.

(61) Hao, T.; Li, J.; Yao, F.; Dong, D.; Wang, Y.; Yang, B.; Wang, C. Injectable Fullerenol/Alginate Hydrogel for Suppression of Oxidative Stress Damage in Brown Adipose-Derived Stem Cells and Cardiac Repair. *ACS Nano* **2017**, *11* (6), 5474–5488.

(62) Wassenaar, J. W.; Braden, R. L.; Osborn, K. G.; Christman, K. L. Modulating in Vivo Degradation Rate of Injectable Extracellular Matrix Hydrogels. *J. Mater. Chem. B* **2016**, *4* (16), 2794–2802.

(63) Singelyn, J. M.; Sundaramurthy, P.; Johnson, T. D.; Schup-Magoffin, P. J.; Hu, D. P.; Faulk, D. M.; Wang, J.; Mayle, K. M.; Bartels, K.; Salvatore, M.; Kinsey, A. M.; Demaria, A. N.; Dib, N.; Christman, K. L. Catheter-Deliverable Hydrogel Derived from Decellularized Ventricular Extracellular Matrix Increases Endogenous Cardiomyocytes and Preserves Cardiac Function Post-Myocardial Infarction. *J. Am. Coll. Cardiol.* **2012**,

59 (8), 751–763.

(64) Wassenaar, J. W.; Gaetani, R.; Garcia, J. J.; Braden, R. L.; Luo, C. G.; Huang, D.; Demaria, A. N.; Omens, J. H.; Christman, K. L. Evidence for Mechanisms Underlying the Functional Benefits of a Myocardial Matrix Hydrogel for Post-MI Treatment. *J. Am. Coll. Cardiol.* **2016**, *67* (9), 1074–1086.

(65) Rane, A. A.; Chuang, J. S.; Shah, A.; Hu, D. P.; Dalton, N. D.; Gu, Y.; Peterson, K. L.; Omens, J. H.; Christman, K. L. Increased Infarct Wall Thickness by a Bio-Inert Material Is Insufficient to Prevent Negative Left Ventricular Remodeling after Myocardial Infarction. *PLoS One* **2011**, *6* (6).

(66) Famili, A.; Kahook, M. Y.; Park, D. A Combined Micelle and Poly(Serinol Hexamethylene Urea)-Co-Poly(N-Isopropylacrylamide) Reverse Thermal Gel as an Injectable Ocular Drug Delivery System. *Macromol. Biosci.* **2014**, *14* (12), 1719–1729.

(67) Vunjak-Novakovic, G.; Tandon, N.; Godier, A.; Maidhof, R.; Marsano, A.; Martens, T. P.; Radisic, M. Challenges in Cardiac Tissue Engineering. *Tissue Eng. Part B-Reviews* **2009**, *16* (October 2016), 169–187.

(68) Severs, N. J.; Coppen, S. R.; Dupont, E.; Yeh, H. I.; Ko, Y. S.; Matsushita, T. Gap Junction Alterations in Human Cardiac Disease. *Cardiovasc. Res.* **2004**, *62* (2), 368–377.

(69) Severs, N. J.; Bruce, A. F.; Dupont, E.; Rothery, S. Remodelling of Gap Junctions and Connexin Expression in Diseased Myocardium. *Cardiovasc. Res.* **2008**, *80* (1), 9–19.

(70) Kostin, S.; Dammer, S.; Hein, S.; Klovekorn, W. P.; Bauer, E. P.; Schaper, J. Connexin 43 Expression and Distribution in Compensated and Decompensated Cardiac Hypertrophy in Patients with Aortic Stenosis. *Cardiovasc. Res.* **2004**, *62* (2), 426–436.

TOC.